ELSEVIER

Journal of Hepatology 49 (2008) 946–954

Journal of Hepatology

www.elsevier.com/locate/jhep

Expression of multidrug resistance-associated protein 3 and cytotoxic T cell responses in patients with hepatocellular carcinoma☆

Eishiro Mizukoshi, Masao Honda, Kuniaki Arai, Tatsuya Yamashita, Yasunari Nakamoto, Shuichi Kaneko*

Department of Gastroenterology, Graduate School of Medicine, Kanazawa University, Kanazawa, Ishikawa 920-8641, Japan

***Background/Aims*: Multidrug resistance-associated protein 3 (MRP3) is a carrier-type transport protein belonging to the ABC transporters. It is expressed in normal tissues, and enhanced expression in many cancers has been reported. In this study, we investigated the usefulness of MRP3 as a target antigen in immunotherapy for hepatocellular carcinoma (HCC).**

***Methods*: The MRP3 expression level in HCC tissue was measured by quantitative PCR. MRP3-specific T cell responses were investigated by several immunological techniques using peripheral blood mononuclear cells or tumor-infiltrating lymphocytes.**

***Results*: The MRP3 expression level in HCC tissue was significantly higher than that in non-cancerous tissue ($P < 0.05$). MRP3-specific cytotoxic T cells (CTLs) could be induced regardless of liver function, the presence or absence of HCV infection, the blood AFP level, and the stage of HCC. The CTLs showed cytotoxicity against HCC cells overexpressing MRP3. A negative correlation was present between the MRP3 expression level in HCC tissue and the frequency of MRP3-specific CTLs. The frequency of MRP3-specific CTLs increased after HCC treatment, such as transcatheter arterial embolization and radiofrequency ablation.**

***Conclusions*: Our study demonstrates that MRP3 is a potential candidate for tumor antigen with strong immunogenicity in HCC immunotherapy.**

© 2008 European Association for the Study of the Liver. Published by Elsevier B.V. All rights reserved.

Keywords: **Immune response; CD8; HLA-A24; Hepatitis; Cancer**

1. Introduction

Hepatocellular carcinoma (HCC) is treatable by hepatectomy or percutaneous ablation when the lesion is localized to some extent, and radical therapeutic effects can be obtained when the resection or cauterization with a safety margin can be performed [1,2]. However, active hepatitis and cirrhosis in the surrounding non-tumor liver tissues exhibit high carcinogenetic potentials to develop *de novo* HCC, and therefore, the recurrence rate of HCC after treatment is very high [3,4].

To protect against recurrence, tumor antigen-specific immunotherapy is an attractive strategy. For the development of HCC-specific immunotherapy and analysis of immune responses to the treatment, the identification of HCC-specific tumor antigens or their antigenic epitopes is necessary. However, only a few HCC-specific tumor antigens and their antigenic epitopes have been identified [5–10].

MRP3 is a carrier-type transport protein belonging to the ABC transporters that transport substances against

Received 11 January 2008; received in revised form 23 April 2008; accepted 7 May 2008; available online 5 June 2008

Associate Editor: V. Barnaba

☆ The authors declare that they do not have anything to disclose regarding funding from industries or conflict of interest with respect to this manuscript.

* Corresponding author. Tel.: +81 76 265 2230; fax: +81 76 234 4250.

E-mail address: skaneko@m-kanazawa.jp (S. Kaneko).

Abbreviations: HLA, human leukocyte antigen; IFN, interferon; PBMC, peripheral blood mononuclear cell; TIL, tumor-infiltrating lymphocytes; HCV, hepatitis C virus; ELISPOT, enzyme linked immunospot.

0168-8278/$34.00 © 2008 European Association for the Study of the Liver. Published by Elsevier B.V. All rights reserved.
doi:10.1016/j.jhep.2008.05.012

the concentration gradient in an ATP energy-dependent manner [11]. It is expressed at a high level in the small and large intestine, pancreas, placenta, and adrenal cortex [12], and recent studies have reported that its expression is enhanced in various cancer cells [13–15]. Yamada et al. demonstrated that MRP3 was a tumor rejection antigen recognized by cytotoxic T cells (CTLs), using lymphocytes infiltrating into lung adenocarcinoma, and identified its CTL epitope [13]. These reports suggest that MRP3 may be useful as a target antigen in HCC immunotherapy. However, the MRP3 expression level in HCC tissue has been controversial [16,17], and the association between the expression level and the degree of the immune response to MRP3 in HCC patients has not been clarified.

In this study, we measured the MRP3 expression level in various hematoma cell lines and HCC tissues in HCC patients, and analyzed immune responses to MRP3 using peripheral blood mononuclear cells (PBMCs) and tumor-infiltrating lymphocytes (TILs) to investigate the usefulness of MRP3 in HCC immunotherapy.

2. Materials and methods

2.1. Patients

This study examined 103 HLA-A24-positive patients with HCC (Table 1). All subjects were negative for Abs to human immunodeficiency virus (HIV), and gave written informed consent to participate in this study in accordance with the Helsinki declaration. The diagnosis of HCC was histologically confirmed by taking US-guided needle biopsy specimens in 35 cases, surgical resection in 13 cases, and autopsy in 4 cases. For the remaining 51 patients, the diagnosis was based on typical hypervascular tumor staining on angiography in addition to typical findings, which showed hyperattenuated areas in the early phase and hypoattenuation in the late phase on dynamic CT [18]. Eleven healthy blood donors with HLA-A24, who did not have a history of cancer and were negative for HBsAg and anti-HCVAb, served as controls.

2.2. Laboratory and virologic testing

Blood samples were tested for HBsAg and HCVAb by commercial immunoassays (Fuji Rebio, Tokyo, Japan). HLA-based typing of PBMC from patients and normal donors was performed as previously described [10].

The serum AFP level was measured by enzyme immunoassay (AxSYM AFP, Abbott Japan, Tokyo, Japan) and the pathological grading of tumor cell differentiation was assessed according to the general rules for the clinical and pathologic study of primary liver cancer [19]. The severity of liver disease (stage of fibrosis) was evaluated according to the criteria of Desmet et al. [20] using biopsy specimens of liver tissue, where F4 was defined as cirrhosis.

2.3. Cell lines

Eight human hepatoma cell lines: HepG2, Alex, Huh6, HLE, HLF, Hep3B, SKHep1, and Huh7, were cultured in DMEM (Gibco, Grand Island, NY, USA) with 10% fetal calf serum (FCS) (Gibco, Grand Island, NY, USA). The HLA-A*2402 gene-transfected C1R cell line (C1R-A24) [21] was cultured in RPMI 1640 medium containing 10% FCS and 500 μg/ml of hygromycin B (Sigma, St. Louis, MO, USA), and K562 was cultured in RPMI 1640 medium containing 10% FCS.

2.4. Quantitative real time detection (RTD)-PCR

We performed quantitative RTD-PCR using TaqMan Universal Master Mix (PE Applied Biosystems, Foster City, CA, USA). Primer pairs and probes for MRP3 and β-actin were obtained from TaqMan assay reagents library. Total RNA was isolated from cell lines and liver tissue samples using an RNA extraction kit (Micro RNA Extraction Kit, Stratagene, La Jolla, CA, USA). We reverse-transcribed 1 μg of isolated RNA to cDNA using SuperScript® II RT (Invitrogen, Carlsbad, CA, USA) according to the manufacturer's instructions, and the resultant cDNA was amplified with appropriate TaqMan assay reagents as previously described [22].

2.5. Preparation of PBMCs and TILs

PBMCs and TILs were isolated as previously described [9]. Fresh PBMCs were used for the CTL induction, and the remaining PBMCs and TILs were resuspended in RPMI 1640 medium containing 80% FCS and 10% dimethyl sulfoxide and cryopreserved until used. In patients with treatment, PBMCs were obtained before and 2–4 weeks after the treatment.

2.6. CTL induction and cytotoxicity assay

Peptides $MRP3_{503}$, $MRP3_{692}$, and $MRP3_{765}$, which were identified to contain a HLA-A24 restricted CTL epitope [13], were used for the induction of MRP3-specific T cells (Table 2). Peptides were synthesized at Mimotope (Melbourne, Australia) and Sumitomo Pharmaceuticals (Osaka, Japan). They were identified using mass spectrometry, and their purities were determined to be >80% by analytical HPLC. CTLs were expanded from PBMCs as previously described [23]. Briefly, four hundred thousand cells per well were stimulated with synthetic peptides at 10 μg/ml, 10 ng/ml rIL-7 and 100 pg/ml rIL-12 (Sigma, St. Louis, Mo) in RPMI 1640 supplemented with 10% heat inactivated human AB serum, 100 U/ml penicillin and 100 μg/ml streptomycin. The cultures were re-stimulated with 10 μg/ml peptide, 20 U/ml rIL-2 (Sigma, St. Louis, MO) and 10^5 mytomicin C treated autologous PBMCs on days 7 and 14. On days 3, 10 and 17, 100 μl of RPMI with 10% human AB serum and 10 U/ml rIL-2 (final concentration) was added to each well.

C1R-A24 cells and human hepatoma cell lines were used as target cells. Cytotoxicity assays were performed in at least 10 HCC patients for each peptide as previously described [10]. Spontaneous release

Table 1
Characteristics of the patients studied

Clinical diagnosis	No. of patients	Sex M/F	Age (yr) Mean ± SD	ALT (IU/L) Mean ± SD	AFP (ng/ml) mean ± SD	Etiology (B/C/B + C/Others)	Child Pugh (A/B/C)	Dif. degree[a] (Wel/Mod/Por/ND)	Tumor size[b] (Large/Small)	Tumor multiplicity (Multiple/Solitary)	Vascular Invasion (+/−)	TNM stage (I/II/IIIA/IIIB/IIIC/IV)
HCC paticnts	103	79/24	63 ± 10	65 ± 37	3155 ± 15946	19/73/2/9	61/39/3	17/31/4/51	79/24	73/30	30/73	24/51/16/1/3/8
Normal donors	11	8/3	35 ± 2	ND	ND	ND	ND	ND	ND	ND	ND	ND

[a] Histological degree of HCC; wel: well-differentiated, mod: moderately differentiated, por: poorly differentiated, ND: not determined.
[b] Tumor size was divided into either 'small' (≤2 cm) or 'large' (>2 cm).

Table 2
Peptides

Peptide	Source	Start position	Amino acid sequence	HLA restriction
$MRP3_{503}$	MRP3	503	LYAWEPSFL	HLA-A24
$MRP3_{692}$	MRP3	692	AYVPQQAWI	HLA-A24
$MRP3_{765}$	MRP3	765	VYSDADIFL	HLA-A24
HIV env_{584}	HIV envelope	584	RYLRDQQLL	HLA-A24
CMV $pp65_{328}$	CMV pp65	328	QYDPVAALF	HLA-A24
AFP_{403}	AFP	403	KYIQESQAL	HLA-A24

was <15% of the maximum release for all experiments. For the assay using hepatoma cell lines, the cytotoxic activity was considered positive when it was higher than that of CTL against K562 which shows non-specific lysis. The assay was performed at least three times for each peptide.

2.7. ELISPOT assay

ELISPOT assays were performed as previously described with the following modifications [9,10]. Peptides $MRP3_{503}$, $MRP3_{692}$, and $MRP3_{765}$ were used for the detection of MRP3-specific T cells. Negative controls consisted of a HIV envelope-derived peptide ($HIVenv_{584}$) [24]. Positive controls consisted of 10 ng/ml phorbol 12-myristate 13-acetate (PMA, Sigma) or a CMV pp65-derived peptide ($CMVpp65_{328}$) [25]. The colored spots were counted with a KS ELISpot Reader (Zeiss, Tokyo, Japan). The number of specific spots was determined by subtracting the number of spots in the absence of antigen from the number of spots in its presence. Responses for peptides $MRP3_{503}$, $MRP3_{692}$, and $MRP3_{765}$ in HCC patients were considered positive if more than the mean + 3SD specific spots in healthy normal donors were detected and if the number of spots in the presence of antigen was at least twofold greater than the number of spots in its absence. Responses for peptides $HIVenv_{584}$ and $CMVpp65_{328}$ were considered positive if more than 10 specific spots were detected and if the number of spots in the presence of antigen was at least twofold greater than the number of spots in the absence of antigen.

2.8. Tetramer staining and flow cytometry

Peptide $MRP3_{765}$ specific tetramer was purchased from Medical Biological Laboratories Co., Ltd (Nagoya, Japan). Tetramer staining was performed according to a previously reported method with several modifications [10]. In brief, PBMCs were stained with CD8-PerCP (BD PharMingen, San Diego, CA, USA) and tetramer-PE (10 μl) for 30 min at room temperature. Cells were washed, fixed with 0.5% paraformaldehyde/PBS, and analyzed on a FACSCalibur™ flow cytometer. Data analysis was undertaken with CELLQuest™ software (Becton–Dickinson, San Jose, CA, USA).

2.9. Statistical analysis

Data are expressed as means ± SD. The χ^2 test with Yates' correction, Fisher's exact probability test, and the unpaired t-test were used for statistical analyses where appropriate. Linear regression lines for the relationship between expression of MRP3 mRNA and MRP3-specific immune responses were calculated using Pearson's correlation coefficient. A level of $P < 0.05$ was considered significant.

3. Results

3.1. Patient profile

The clinical profiles of the patients are shown in Table 1. In 52 patients, HCC was histologically classified as well-, moderately, and poorly differentiated HCC in 17, 31, and 4, respectively. In the other patients, HCC was diagnosed based on typical CT findings and AFP elevation. On tumor classification based on the size and number, the tumor was large (>2 cm) in 79, small (≤2 cm) in 24, multiple in 73, and solitary in 30. Vascular invasion was noted in 30 patients. On tumor classification using the TNM staging of the Union Internationale Contre Le Cancer (UICC) classification system (6th version), 24, 51, 16, 1, 3, and 8 patients were staged I, II, IIIA, IIIB, IIIC, and IV, respectively.

3.2. Expression of MRP3 in hepatoma cell lines and HCC tissues

To investigate the MRP3 expression level in HCC, we measured MRP3 mRNA in 8 hepatoma cell lines by real-time PCR. The expression ratio of MRP3 to β-actin, measured as an internal control, is shown in Fig. 1A. All hepatoma cell lines except HLF expressed MRP3, but the expression level varied among the cell lines. HepG2, Hep3B and Huh7 showed high expression levels, but Alex, HLE, SKHep1 and Huh6 showed low expression levels.

The MRP3 expression level in HCC tissues was compared with non-cancerous tissues in specimens obtained from 20 HCC patients by US-guided needle tumor biopsy or surgical resection. The MRP3 expression level was significantly higher in HCC tissue than in the non-cancerous tissue ($P < 0.05$) (Fig. 1B). In the analysis of the individual MRP3 expression levels, 11 of 20 (55%) HCC tissues showed higher expression level than that of Huh 7 whose average of expression level is 1.0 (Fig. 1C).

3.3. Cytotoxic activity of MRP3 peptide-specific CTL against hepatoma cell lines

Whether the MRP3-derived peptides used were capable of inducing peptide-specific CTL from PBMCs was investigated in at least 10 HCC patients. The CTLs specific for $MRP3_{503}$, $MRP3_{692}$, and $MRP3_{765}$ were induced in 3, 3 and 2 patients, respectively. As shown in Fig. 2A, all CTL induced with $MRP3_{503}$, $MRP3_{692}$, and $MRP3_{765}$ showed high-level cytotoxicity against C1RA24 cells pulsed with the corresponding peptides.

These CTLs exhibited cytotoxicity against hepatoma cell lines with the HLA-A24 molecule and high expression of MRP3, HepG2 and HLE, but not against MRP3-hypoexpressing Huh6 and MRP3-overexpressing Huh7 without HLA-A24 molecule (Fig. 2B).

3.4. T Cell responses to MRP3-derived peptides assessed by IFN-γ ELISPOT analysis

To determine a significant number of T cells that specifically reacted with $MRP3_{503}$, $MRP3_{692}$ and $MRP3_{765}$

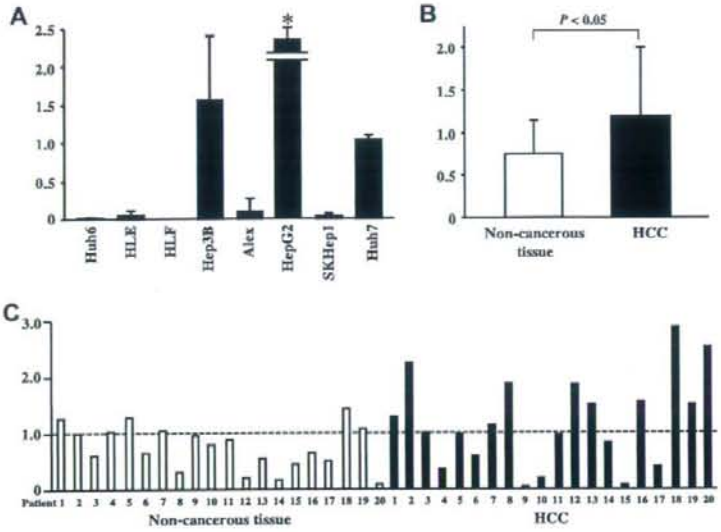

Fig. 1. Expression levels of MRP3 mRNA. (A) Expression of MRP3 mRNA was measured by real-time PCR in hepatoma cell lines. (B) Comparison of MRP3 mRNA expression levels between non-tumor (white bar) and tumor (solid bar) tissues. The data are expressed as means + SD. The unpaired *t*-test was used for a statistical analysis. (C) Comparison of MRP3 mRNA expression levels between non-tumor (white bar) and tumor (solid bar) tissues in individual HCC patients. * denotes 6.15 + 4.21.

peptides in HCC patients, ELISPOT assays were performed using PBMCs from 11 healthy donors. The number of specific spots was 0.2 ± 0.5, 1.5 ± 2.1, 0.9 ± 1.0, 1.3 ± 2.0, and 13.3 ± 15.7 cells/3×10^5 PBMCs, respectively (Fig. 3). Similarly, cells that specifically reacted with the peptides were counted in HCC patient-derived PBMCs. Regarding a number of T cells that specifically reacted with the peptide of larger than the mean + 3SD of that in healthy donor-derived PBMCs as a significant response, 20.0, 14.1, and 21.4% of the patients showed significant responses to $MRP3_{503}$, $MRP3_{692}$, and $MRP3_{765}$, respectively (Fig. 4A). A significant response specific for $CMVpp65_{328}$ was detected in 51.0% and 36.4% of the HCC patients and healthy donors, respectively, showing no significant difference between the 2 groups. On the other hand, no significant response for $HIVenv_{584}$ was observed in both groups.

On similar analysis of TIL, 75.0, 75.0, and 37.5% of the patients showed significant responses to $MRP3_{503}$, $MRP3_{692}$, and $MRP3_{765}$, respectively, revealing that the frequencies were higher than those in PBMCs (Fig. 4B).

3.5. Detection of $MRP3_{765}$ tetramer$^+$ and CD8$^+$ T lymphocytes in PBMCs

The frequency of MRP3-specific T cells was also investigated using $MRP3_{765}$ tetramer in 20 HCC patients. To confirm the specificity of $MRP3_{765}$ tetramer, we tried to detect the tetramer$^+$ cells in a CTL line induced by stimulation with $MRP3_{765}$ peptide. The frequency of $MRP3_{765}$ tetramer$^+$ cells in CD8$^+$ cells was increased from 0.03% before to 9.15% after stimulation (Fig. 5A). When PBMC was stimulated with irrelevant peptide (AFP_{403}), the frequency of $MRP3_{765}$ tetramer$^+$ cells was only 0.08%.

To count the frequency of tetramer$^+$ cells in peripheral blood, we used freshly isolated non-stimulated PBMCs for the assay. The tetramer$^+$ and CD8$^+$ T cells accounted for 0.00–0.23% in PBMCs of HCC patients (Fig. 5B). Next, the results were compared with those of ELISPOT assay. In patients 1 to 7, both $MRP3_{765}$ tetramer$^+$ and IFN-γ producing cells responding to the peptide in ELISPOT assay were detected. In contrast, in patients 8 to 13, the frequency of tetramer$^+$ cells was high, but no significant increase in the $MRP3_{765}$ peptide-specific T cell count was detected by the ELISPOT assay.

3.6. MRP3-specific T cell responses and clinical features of HCC patients

To clarify the clinical characteristics of MRP3-specific T cell responses in HCC patients, the clinical background was compared between patients who showed positive responses to MRP3-derived peptides on ELISPOT assay and those who did not. No significant differences were noted between the 2 groups (Table 3).

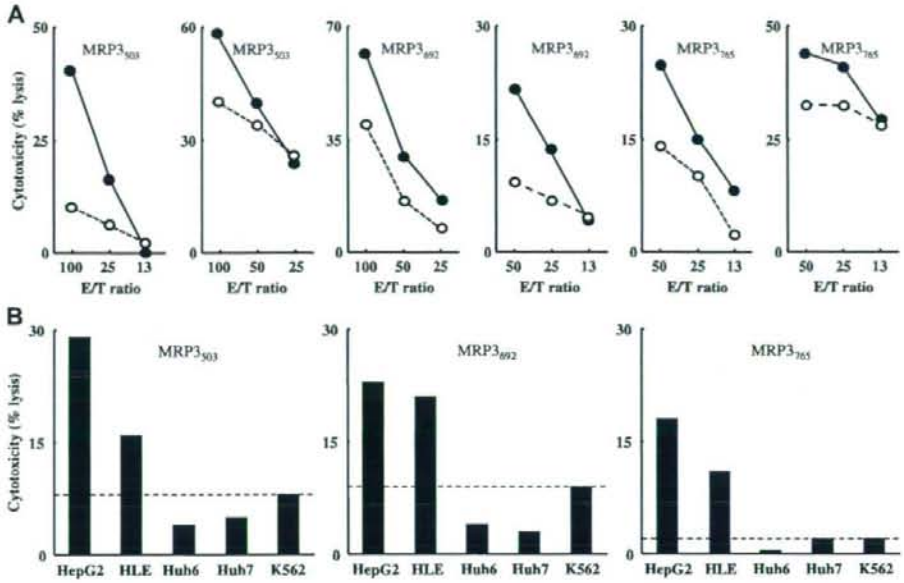

Fig. 2. Cytotoxicity of MRP3-specific T-cell lines derived with peptide in patients with HCC. (A) The cytotoxicity of T-cell lines was determined by a standard 6-h cytotoxicity assay at various effector to target (E/T) ratios against C1R-A*2402 cells pulsed with or without one of the MRP3-derived peptides listed in Table 2. The open circle shows the cytotoxicity against C1R-A*2402 cells pulsed without a peptide. The closed circle shows the cytotoxicity against C1R-A*2402 cells pulsed with a peptide. (B) Cytotoxicity of MRP3-specific T-cell lines derived with peptide was also measured against hepatoma cell lines. The cytotoxicity was considered positive when it was higher than that against K562 which shows non-specific lysis. HepG2 expresses MRP3 and has HLA-A*2402. Huh 6 and HLE show a low expression of MRP3 and have HLA-A*2402. Huh 7 shows MRP3 expression, but does not have HLA-A*2402. Cytotoxicity was determined by a standard 6-h cytotoxic assay (E/T ratio of 50:1).

In 20 HCC patients in whom the MRP3 expression level in HCC tissue could be measured, the relationship between the expression level and frequency of MRP3-specific T cells was investigated. A significant negative correlation was present between the MRP3 expression level in HCC tissue and MRP3-specific T cell frequency ($r = -0.54$, $P < 0.05$) (Fig. 6A). When the relationship between the MRP3 expression level in HCC tissue and CMVpp65-specific T-cell frequency was similarly analyzed, no significant correlation was present. Furthermore, when the patients were divided into groups with high and low HCC tissue MRP3 expression levels, setting the border to the mean MRP3 expression level in the normal liver tissues, 0.743, the peripheral blood MRP3-specific T cell frequency was significantly higher in the low- than in the high-level group ($p < 0.05$) (Fig. 6B). The CMVpp65-specific T cell frequency was not significantly different between the 2 groups.

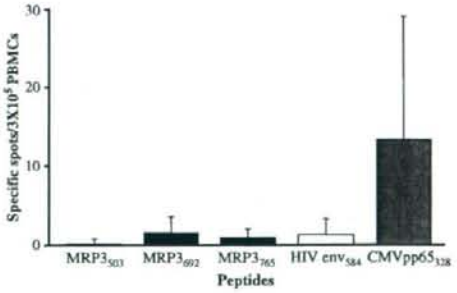

Fig. 3. Direct ex-vivo analysis (IFN-γ ELISPOT assay) of peripheral blood T cell responses to MRP3-derived peptides (peptides $MRP3_{503}$, $MRP3_{692}$, and $MRP3_{765}$: solid bars) or control peptides (peptides $HIVenv_{584}$ and $CMVpp65_{328}$: open and grey bars, respectively) in healthy normal donors. The data are expressed as means + SD.

3.7. Enhancement of MRP3-specific T cell responses after anti-cancer treatment

Several studies including our report have clarified that HCC treatment enhanced HCC-specific immune responses [9,26,27]. We investigated whether MRP3-specific T cell responses observed in HCC patients were enhanced by HCC treatment. In 12 patients who underwent TAE or radiofrequency ablation (RFA) or both

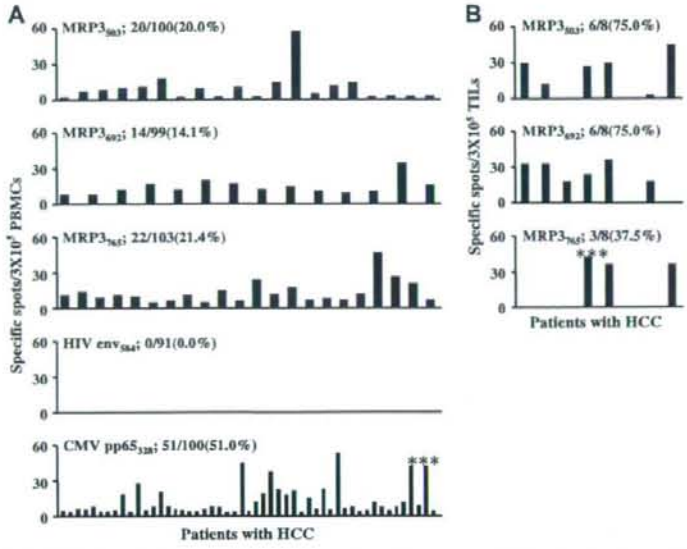

Fig. 4. Direct ex-vivo analysis (IFN-γ ELISPOT assay) of PBMCs (A) and TILs (B) response to MRP3-derived peptides (peptides $MRP3_{503}$, $MRP3_{692}$, and $MRP3_{765}$) or control peptides (peptides $HIVenv_{584}$ and $CMVpp65_{328}$) in HCC patients. Only significant IFN-γ responses are included. Responses to peptides $MRP3_{503}$, $MRP3_{692}$, and $MRP3_{765}$ were considered positive if more than the mean + 3SD specific spots in healthy normal donors were detected and if the number of spots in the presence of antigen was at least twofold greater than that in its absence. Responses to peptides $HIVenv_{584}$ and $CMVpp65_{328}$ were considered positive if more than 10 specific spots were detected and if the number of spots in the presence of antigen was at least twofold greater than that in its absence. The peptide sequences are described in Table 2. * denotes 770 specific spots. ** denotes 210 specific spots. * denotes 72 specific spots.**

without MRP3-specific T-cell responses before treatment, changes in the MRP3-specific T cell frequency were investigated by measuring the frequency by ELISPOT assay before and after treatment. The $MRP3_{503}$, $MRP3_{692}$, or $MRP3_{765}$ peptide-specific T cell frequency was increased after treatment in 8 of the 12 patients (Table 4). In contrast, the immune response to $HIVenv_{584}$ peptide was not enhanced in any patient, and that to $CMVpp65_{328}$ peptide was enhanced in one patient.

4. Discussion

The expression of MRP3 has been reported in several normal tissues and cancer cells [14,15,28,29]. Although MRP3 expression in HCC tissue was confirmed by immunohistochemical staining [16], the expression level varied among patients, and a conclusion has not been reached as to whether the expression is increased compared to that in normal liver tissue [16,17]. In this study, MRP3 expression in HCC tissue was detected in all 20 HCC patients, and the expression level was significantly higher than that in non-cancerous tissue.

The presence of MRP3-recognizing CTL has been reported in lung, colon, bladder, and renal cancer patients [13,30]. However, to our knowledge, there is no report showing the presence of MRP3-specific CTL in HCC patients. In this study, we showed that MRP3-specific CTL could be induced by stimulating PBMCs with MRP3-derived peptides, and the induced CTL showed cytotoxicity against hepatoma cell lines overexpressing MRP3. Based on these findings, we confirmed that MRP3-specific CTLs exist in HCC patients and MRP3 serves as an immunogenic antigen in HCC.

The frequency of peripheral blood CTL specific to each MRP3 epitope was similar to the reported frequencies of CTL against other tumor antigen epitopes [9,10,31–33]. The CTLs were induced even in an early stage of HCC and regardless of HCV infection. In TILs, MRP3-specific CTL were more frequently detected, compared to that in peripheral blood, suggesting that MRP3-specific CTL are not only present in peripheral blood but also infiltrate into the tumor.

The presence and frequency of MRP3-specific CTL were also confirmed using $MRP3_{765}$ tetramer. However, MRP3-specific CTL could not be detected by ELISPOT assay in 6 patients despite a high frequency being

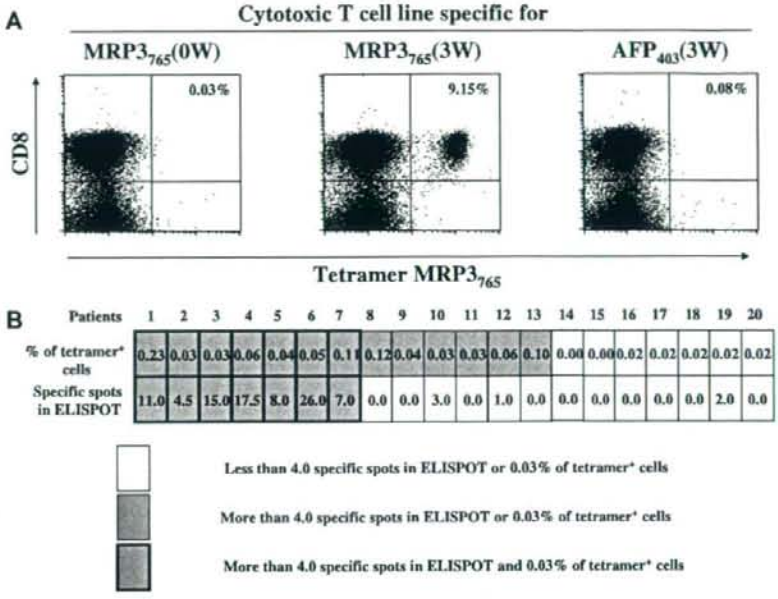

Fig. 5. Detection of MRP3-specific, HLA-A*2402-tetramer+ and CD8+ T lymphocytes in the peripheral blood. (A) Specificity of the $MRP3_{765}$ tetramer was confirmed by staining peptide-specific and non-specific in vitro-expanded T-cell lines. (B) Analysis of the association between the frequency of tetramer+ cells and IFN-γ-producing cells detected on ELISPOT assay was performed in 20 patients.

detected by the tetramer. These findings were similar to those of hTERT-specific CTL in our previous study [10], suggesting the presence of MRP3-specific non-functional T cells in HCC patients.

In the analysis of association between the HCC tissue MRP3 expression level and MRP3-specific T-cell frequency in peripheral blood, a negative correlation was detected, suggesting that MRP3-specific immune responses exert an immune pressure on MRP3-expressing HCC cells. Recent studies have shown the involvement of MRP3 in the resistance to anti-tumor drugs and poor prognosis in several cancer patients [14,15,28,29,34,35]. Taken together with these reports, our results suggest the possibility that MRP3-targeting immunotherapy not only simply eliminates cancers but also improves drug resistance and the prognosis by inhibiting MRP3 expression in cancer cells.

Further to evaluate the usefulness of MRP3 in HCC immunotherapy, we also investigated the association between HCC treatment and the MRP3-specific CTL frequency. As we and other groups previously reported [9,26,27], the MRP3-specific CTL frequency was increased after treatment in 8 of the 12 patients in whom no immune response to MRP3 was detected before treatment, whereas the HIV env_{584}- and $CMVpp65_{328}$-specific CTL frequencies were not increased, excluding one patient, suggesting that this phenomenon represents the enhancement of MRP3-specific immune responses. These findings also confirmed that MRP3 is an antigen expressed in HCC tis-

Table 3
Univariate analysis of the effect of variables on the T cell response against MRP3

	Patients with positive T cell response	Patients without positive T cell response	p-value[a]
No. of patients	38	65	
Age (years)[b]	61.4 ± 10.0	64.3 ± 9.7	NS
Sex (M/F)	30/8	49/16	NS
AFP level (≤20/>20)	17/21	21/44	NS
Diff. degree of HCC (well/moderate or poor/ND)[c]	5/14/19	12/21/32	NS
Tumor multiplicity (multiple/solitary)	30/8	43/22	NS
Vascular invasion (+/−)	12/26	18/47	NS
TNM factor			
(T1/T2–4)	6/32	18/47	NS
(N0/N1)	36/2	64/1	NS
(M0/M1)	36/2	57/8	NS
TNM stage (I/II–IV)	6/32	18/47	NS
Histology of non-tumor liver (LC/chronic hepatitis)	30/8	55/10	NS
Liver function (Child A/B/C)	23/14/1	38/25/2	NS
Etiology (HCV/HBV/others)	26/7/5	49/12/4	NS

[a] NS, not significant.
[b] Data are expressed as means ± SD.
[c] ND, not determined.

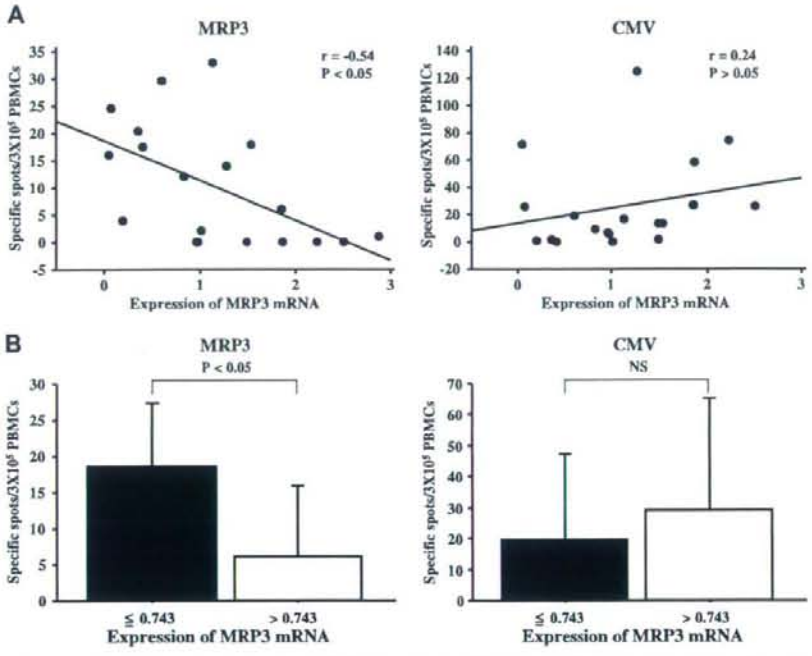

Fig. 6. Analysis of the association between the frequencies of MRP3- specific T cells detected on ELSPOT assay and the expression levels of MRP3 mRNA in HCC tissues. The frequency of MRP3-specific T cells was calculated by the sum of specific spots against $MRP3_{503}$, $MRP3_{692}$, and $MRP3_{765}$ peptides. (A) Linear regression lines for the relationship between the expression of MRP3 mRNA and the frequency of MRP3- or CMVpp65-specific T cells were calculated using Pearson's correlation coefficient. (B) Analysis of the frequency of MRP3- or CMVpp65-specific T cells in patients with low and high expression levels of MRP3 mRNA in HCC tissues.

sue, and has strong immunogenicity that readily induces CTL in vivo.

In conclusion, our study demonstrates that MRP3 is a potential candidate for tumor antigen with strong immunogenicity in HCC immunotherapy.

Acknowledgements

The authors thank Maki Kawamura, Kazumi Fushimi, Nami Nishiyama and Mikiko Nakamura for technical assistance.

Table 4
T cell response to MRP3-derived peptides by ELISPOT assay before and after treatment

	Treatment[a]	Before treatment					After treatment				
		$MRP3_{503}$	$MRP3_{692}$	$MRP3_{765}$	$HIVenv_{584}$	$CMVpp65_{328}$	$MRP3_{503}$	$MRP3_{692}$	$MRP3_{765}$	$HIVenv_{584}$	$CMVpp65_{328}$
Patient 1	TAE + RF	1	0	0	0	9	**5**	5	3	2	6
Patient 2	TAE + RF	0	0	0	0	0	**2**	2	0	0	2
Patient 3	TAE + RF	0	2	0	4	5	**8**	1	**6**	2	**13**
Patient 4	TAE + RF	0	0	0	0	**16**	0	0	0	0	**46**
Patient 5	TAE + RF	0	4	0	1	3	**5**	0	**37**	0	ND[b]
Patient 6	TAE + RF	0	0	0	0	**61**	0	0	4	1	**59**
Patient 7	TAE	0	0	0	0	**92**	0	0	**6**	0	**139**
Patient 8	TAE	0	1	0	1	9	0	1	0	0	0
Patient 9	RF	0	0	0	0	**74**	**6**	7	2.5	2.5	**65**
Patient 10	RF	0	0	0	0.5	0	**3**	0	1	0.5	9.5
Patient 11	RF	1.5	0	1	1	9.5	0	3	**9.5**	1	5.5
Patient 12	RF	0	0	0	0	**13**	0	0	0	0	6

Bold and underlined letters indicate a significant increase as described in materials and methods.

[a] TAE, transcatheter arterial embolization; RF, radiofrequency ablation.

[b] ND: not determined.

References

[1] Llovet JM, Burroughs A, Bruix J. Hepatocellular carcinoma. Lancet 2003;362:1907–1917.

[2] Lin SM, Lin CJ, Lin CC, Hsu CW, Chen YC. Radiofrequency ablation improves prognosis compared with ethanol injection for hepatocellular carcinoma < or =4 cm. Gastroenterology 2004;127:1714–1723.

[3] Ercolani G, Grazi GL, Ravaioli M, Del Gaudio M, Gardini A, Cescon M, et al. Liver resection for hepatocellular carcinoma on cirrhosis: univariate and multivariate analysis of risk factors for intrahepatic recurrence. Ann Surg 2003;237:536–543.

[4] Omata M, Tateishi R, Yoshida H, Shiina S. Treatment of hepatocellular carcinoma by percutaneous tumor ablation methods: ethanol injection therapy and radiofrequency ablation. Gastroenterology 2004;127:S159–S166.

[5] Butterfield LH, Ribas A, Meng WS, Dissette VB, Amarnani S, Vu HT, et al. T-cell responses to HLA-A*0201 immunodominant peptides derived from alpha-fetoprotein in patients with hepatocellular cancer. Clin Cancer Res 2003;9:5902–5908.

[6] Shang XY, Chen HS, Zhang HG, Pang XW, Qiao H, Peng JR, et al. The spontaneous CD8+ T-cell response to HLA-A2-restricted NY-ESO-1b peptide in hepatocellular carcinoma patients. Clin Cancer Res 2004;10:6946–6955.

[7] Zerbini A, Pilli M, Soliani P, Ziegler S, Pelosi G, Orlandini A, et al. Ex vivo characterization of tumor-derived melanoma antigen encoding gene-specific CD8+cells in patients with hepatocellular carcinoma. J Hepatol 2004;40:102–109.

[8] Komori H, Nakatsura T, Senju S, Yoshitake Y, Motomura Y, Ikuta Y, et al. Identification of HLA-A2- or HLA-A24-restricted CTL epitopes possibly useful for glypican-3-specific immunotherapy of hepatocellular carcinoma. Clin Cancer Res 2006;12:2689–2697.

[9] Mizukoshi E, Nakamoto Y, Tsuji H, Yamashita T, Kaneko S. Identification of alpha-fetoprotein-derived peptides recognized by cytotoxic T lymphocytes in HLA-A24+ patients with hepatocellular carcinoma. Int J Cancer 2006;118:1194–1204.

[10] Mizukoshi E, Nakamoto Y, Marukawa Y, Arai K, Yamashita T, Tsuji H, et al. Cytotoxic T cell responses to human telomerase reverse transcriptase in patients with hepatocellular carcinoma. Hepatology 2006;43:1284–1294.

[11] Borst P, Elferink RO. Mammalian ABC transporters in health and disease. Annu Rev Biochem 2002;71:537–592.

[12] Kiuchi Y, Suzuki H, Hirohashi T, Tyson CA, Sugiyama Y. cDNA cloning and inducible expression of human multidrug resistance associated protein 3 (MRP3). FEBS Lett 1998;433:149–152.

[13] Yamada A, Kawano K, Koga M, Matsumoto T, Itoh K. Multidrug resistance-associated protein 3 is a tumor rejection antigen recognized by HLA-A2402-restricted cytotoxic T lymphocytes. Cancer Res 2001;61:6459–6466.

[14] Tada Y, Wada M, Migita T, Nagayama J, Hinoshita E, Mochida Y, et al. Increased expression of multidrug resistance-associated proteins in bladder cancer during clinical course and drug resistance to doxorubicin. Int J Cancer 2002;98:630–635.

[15] Young LC, Campling BG, Cole SP, Deeley RG, Gerlach JH. Multidrug resistance proteins MRP3, MRP1, and MRP2 in lung cancer: correlation of protein levels with drug response and messenger RNA levels. Clin Cancer Res 2001;7:1798–1804.

[16] Nies AT, Konig J, Pfannschmidt M, Klar E, Hofmann WJ, Keppler D. Expression of the multidrug resistance proteins MRP2 and MRP3 in human hepatocellular carcinoma. Int J Cancer 2001;94:492–499.

[17] Zollner G, Wagner M, Fickert P, Silbert D, Fuchsbichler A, Zatloukal K, et al. Hepatobiliary transporter expression in human hepatocellular carcinoma. Liver Int 2005;25:367–379.

[18] Araki T, Itai Y, Furui S, Tasaka A. Dynamic CT densitometry of hepatic tumors. AJR Am J Roentgenol 1980;135:1037–1043.

[19] Liver cancer study group of Japan. General rules for the clinical and pathological study of primary liver cancer. Second English Edition. Kanehara & Co., Ltd., Tokyo. 2003.

[20] Desmet VJ, Gerber M, Hoofnagle JH, Manns M, Scheuer PJ. Classification of chronic hepatitis: diagnosis, grading and staging. Hepatology 1994;19:1513–1520.

[21] Oiso M, Eura M, Katsura F, Takiguchi M, Sobao Y, Masuyama K, et al. A newly identified MAGE-3-derived epitope recognized by HLA-A24-restricted cytotoxic T lymphocytes. Int J Cancer 1999;81:387–394.

[22] Honda M, Yamashita T, Ueda T, Takatori H, Nishino R, Kaneko S. Different signaling pathways in the livers of patients with chronic hepatitis B or chronic hepatitis C. Hepatology 2006;44:1122–1138.

[23] Mizukoshi E, Nascimbeni M, Blaustein JB, Mihalik K, Rice CM, Liang TJ, et al. Molecular and immunological significance of chimpanzee major histocompatibility complex haplotypes for hepatitis C virus immune response and vaccination studies. J Virol 2002;76:6093–6103.

[24] Ikeda-Moore Y, Tomiyama H, Miwa K, Oka S, Iwamoto A, Kaneko Y, et al. Identification and characterization of multiple HLA-A24-restricted HIV-1 CTL epitopes: strong epitopes are derived from V regions of HIV-1. J Immunol 1997;159:6242–6252.

[25] Kuzushima K, Hayashi N, Kimura H, Tsurumi T. Efficient identification of HLA-A*2402-restricted cytomegalovirus-specific CD8(+) T-cell epitopes by a computer algorithm and an enzyme-linked immunospot assay. Blood 2001;98:1872–1881.

[26] Zerbini A, Pilli M, Penna A, Pelosi G, Schianchi C, Molinari A, et al. Radiofrequency thermal ablation of hepatocellular carcinoma liver nodules can activate and enhance tumor-specific T-cell responses. Cancer Res 2006;66:1139–1146.

[27] Ayaru L, Pereira SP, Alisa A, Pathan AA, Williams R, Davidson B, et al. Unmasking of alpha-fetoprotein-specific CD4(+) T cell responses in hepatocellular carcinoma patients undergoing embolization. J Immunol 2007;178:1914–1922.

[28] Konig J, Hartel M, Nies AT, Martignoni ME, Guo J, Buchler MW, et al. Expression and localization of human multidrug resistance protein (ABCC) family members in pancreatic carcinoma. Int J Cancer 2005;115:359–367.

[29] Steinbach D, Wittig S, Cario G, Viehmann S, Mueller A, Gruhn B, et al. The multidrug resistance-associated protein 3 (MRP3) is associated with a poor outcome in childhood ALL and may account for the worse prognosis in male patients and T-cell immunophenotype. Blood 2003;102:4493–4498.

[30] Komohara Y, Harada M, Arima Y, Suekane S, Noguchi M, Yamada A, et al. Anti-cancer vaccine candidates in specific immunotherapy for bladder carcinoma. Int J Oncol 2006;29:1555–1560.

[31] Nagorsen D, Keilholz U, Rivoltini L, Schmittel A, Letsch A, Asemissen AM, et al. Natural T-cell response against MHC class I epitopes of epithelial cell adhesion molecule, her-2/neu, and carcinoembryonic antigen in patients with colorectal cancer. Cancer Res 2000;60:4850–4854.

[32] Griffioen M, Borghi M, Schrier PI, Osanto S. Detection and quantification of CD8(+) T cells specific for HLA-A*0201-binding melanoma and viral peptides by the IFN-gamma-ELISPOT assay. Int J Cancer 2001;93:549–555.

[33] Rentzsch C, Kayser S, Stumm S, Watermann I, Walter S, Stevanovic S, et al. Evaluation of pre-existent immunity in patients with primary breast cancer: molecular and cellular assays to quantify antigen-specific T lymphocytes in peripheral blood mononuclear cells. Clin Cancer Res 2003;9:4376–4386.

[34] Oguri T, Isobe T, Fujitaka K, Ishikawa N, Kohno N. Association between expression of the MRP3 gene and exposure to platinum drugs in lung cancer. Int J Cancer 2001;93:584–589.

[35] Steinbach D, Lengemann J, Voigt A, Hermann J, Zintl F, Sauerbrey A. Response to chemotherapy and expression of the genes encoding the multidrug resistance-associated proteins MRP2, MRP3, MRP4, MRP5, and SMRP in childhood acute myeloid leukemia. Clin Cancer Res 2003;9:1083–1086.

Available online at www.sciencedirect.com
ScienceDirect
Metabolism Clinical and Experimental 57 (2008) 1071–1077
Metabolism
Clinical and Experimental
www.metabolismjournal.com

Increased oxidative stress precedes the onset of high-fat diet–induced insulin resistance and obesity

Naoto Matsuzawa-Nagata[a,b], Toshinari Takamura[b,*], Hitoshi Ando[b], Seiji Nakamura[a,b], Seiichiro Kurita[b], Hirofumi Misu[b], Tsuguhito Ota[b], Masayoshi Yokoyama[b], Masao Honda[b], Ken-ichi Miyamoto[a], Shuichi Kaneko[b]

[a]*Department of Medicinal Informatics, Kanazawa University Graduate School of Medical Science, Kanazawa, Ishikawa 920-8641, Japan*
[b]*Department of Disease Control and Homeostasis, Kanazawa University Graduate School of Medical Science, Kanazawa, Ishikawa 920-8641, Japan*
Received 27 June 2007; accepted 28 March 2008

Abstract

Insulin resistance is a key pathophysiological feature of metabolic syndrome. However, the initial events triggering the development of insulin resistance and its causal relations with dysregulation of glucose and fatty acids metabolism remain unclear. We investigated biological pathways that have the potential to induce insulin resistance in mice fed a high-fat diet (HFD). We demonstrate that the pathways for reactive oxygen species (ROS) production and oxidative stress are coordinately up-regulated in both the liver and adipose tissue of mice fed an HFD before the onset of insulin resistance through discrete mechanism. In the liver, an HFD up-regulated genes involved in sterol regulatory element binding protein 1c–related fatty acid synthesis and peroxisome proliferator–activated receptor α–related fatty acid oxidation. In the adipose tissue, however, the HFD down-regulated genes involved in fatty acid synthesis and up-regulated nicotinamide adenine dinucleotide phosphate (NADPH) oxidase complex. Furthermore, increased ROS production preceded the elevation of tumor necrosis factor–α and free fatty acids in the plasma and liver. The ROS may be an initial key event triggering HFD-induced insulin resistance.
© 2008 Elsevier Inc. All rights reserved.

1. Introduction

Insulin resistance and obesity are generally brought about by an excessive nutrient condition attributable to an imbalance among energy intake, expenditure, and storage. Importantly, liver and adipose tissue jointly participate in maintaining glucose and lipid homeostasis through the secretion of various humoral factors and/or neural networks [1-3]. Previous studies have validated the presence of molecular signatures typical of the liver and adipose tissue in mouse models of obesity [4] and in mice fed a high-fat diet (HFD) [5]. It is believed that perturbations in these "intertissue communications" may be involved in the development of insulin resistance, obesity, and other features of metabolic syndrome [6]. It remains unclear, however, which factors alter communication among tissues and impair the ability of tissues to adapt to changing metabolic states.

To determine which initial events trigger the development of HFD-induced insulin resistance and obesity, we globally analyzed the biological pathways that are coordinately altered in both the liver and adipose tissue of mice fed an HFD. This was accomplished through the use of microarray and quantitative real-time polymerase chain reaction (PCR) analyses. We found that oxidative stress pathways, which are regulated through the balance of reactive oxygen species (ROS) production and antioxidant enzyme activity [7], are up-regulated in both tissues before the onset of insulin resistance and obesity induced by an HFD.

2. Materials and methods

2.1. Animals and experimental design

Male C57BL/6J mice were purchased from Charles River Laboratories Japan (Yokohama, Japan) at 6 weeks of age. After a 2-week acclimation period, the mice were divided randomly into 2 groups: (*a*) mice given a standard chow containing 5.9%

* Corresponding author. Tel.: +81 76 265 2233; fax: +81 76 234 4250.
E-mail address: ttakamura@m-kanazawa.jp (T. Takamura).

0026-0495/$ – see front matter © 2008 Elsevier Inc. All rights reserved.
doi:10.1016/j.metabol.2008.03.010

fat (in the form of soybean oil) by weight (control, n = 10) and (*b*) mice given an HFD containing 40% fat (in the form of cocoa butter) by weight (HFD, n = 10). Both diets used in this study were prepared by Oriental Yeast (Tokyo, Japan). The mice were housed in a room maintained at a controlled temperature (23°C ± 1°C) and a 12-hour light/12-hour dark cycle. In addition, animals were given free access to water and food. All animal procedures were in accordance with the Guidelines for the Care and Use of Laboratory Animals at the Takara-machi campus of Kanazawa University, Japan.

2.2. Glucose and insulin tolerance tests

For the oral glucose tolerance test (GTT), mice were fasted for 12 hours before glucose was administered at 1.5 g/kg body weight. For the insulin tolerance test (ITT), mice were injected intraperitoneally with insulin (0.5 U/kg body weight, Humulin R; Eli Lilly Japan, Kobe, Japan) after a 4-hour fast. Glucose values were measured in whole venous blood using a blood glucose monitoring system (FreeStyle; Kissei, Matsumoto, Japan) at 0, 15, 30, 60, and 120 minutes after the administration of either glucose or insulin.

2.3. Tissue preparation, blood sampling, and analysis

After a 12-hour fast, blood samples were obtained from the tail vein. Mice were then killed by cervical dislocation under diethyl ether anesthesia. The liver and adipose tissue (retroperitoneal fat) were immediately removed and weighed. A large portion of tissue was snap-frozen in liquid nitrogen for later RNA analysis. Enzymatic assays for total cholesterol, free fatty acids (FFAs), and triglycerides were performed using commercial kits purchased from Wako (Osaka, Japan). The plasma level of tumor necrosis factor (TNF) α was measured with a mouse TNF-α enzyme-linked immunosorbent assay kit (Pierce Biotechnology, Rockford, IL).

2.4. Measurement of hepatic lipid content

Hepatic lipids were extracted with chloroform-methanol (2:1) according to previously published methods [8]. The resulting extract was dissolved in water and subsequently analyzed for triglycerides, total cholesterol, and FFAs using commercial kits (Wako).

2.5. Measurement of oxidative stress in liver and adipose tissue

The concentration of proteins containing carbonyl groups in the liver and retroperitoneal fat (those that react with 2,4-dinitrophenylhydrazine to form the corresponding hydrazone) was determined spectrophotometrically according to commercial kit instructions (protein carbonyl assay kit; Cayman Chemical, Ann Arbor, MI).

2.6. RNA preparation for microarray and hybridization analysis

Total RNA was isolated from the frozen liver and retroperitoneal fat using a ToTALLY RNA kit (Applied Biosystems, Foster City, CA) and an RNeasy Lipid Tissue Mini kit (Qiagen, Germantown, MD), respectively. Each sample was prepared by pooling equal amounts of total RNA from 3 mice of the same experimental or control group. Three micrograms of total RNA was used for the synthesis of amino allyl antisense RNA with an Amino Allyl MessageAmp II aRNA kit (Applied Biosystems). These samples were then used for oligomicroarrays (AceGene Mouse 30K; DNA Chip Research, Yokohama, Japan). The microarray hybridization sample and reference antisense RNA were labeled with Cy5 and Cy3, respectively. Hybridization and washing were performed according to the manufacturer's instructions. The microarray was scanned using a G2505B microarray scanner (Agilent Technologies, Palo Alto, CA), and the image was analyzed using GenePix Pro 4.1 software (Axon Instruments, Union City, CA). An arbitrary cutoff signal value (<50) for both colors was used to filter genes with low expression values. Data were normalized (LOWESS method) using GeneSpring v7.2 software (Agilent Technologies). For pathway analysis, we used the GenMAPP and MAPPFinder software packages (http://www.genmapp.org) [9]. The GenMAPP program contains many pathway maps that can be associated with imported microarray data. The MAPPFinder program, which links gene expression data to the pathway maps, can calculate the *z* score (standardized difference score) and the percentage of genes measured that meet user-defined criteria (±20% in change-fold in our analysis). Using the *z* score and the percentage, the pathways were ranked by the relative amount of gene expression changes.

2.7. Quantitative real-time PCR

Total RNA (100 ng of the same sample used for microarray analysis) was reverse transcribed using random primers and SuperScript II reverse transcriptase (Invitrogen, Carlsbad, CA). The PCR was performed on an ABI PRISM 7900HT (Applied Biosystems). The specific PCR primers and TaqMan probes were obtained from Applied Biosystems. The PCR conditions were one cycle at 50°C for 2 minutes and 95°C for 10 minutes, followed by 40 cycles at 95°C for 15 seconds and 60°C for 1 minute.

2.8. Statistical analysis

All results are reported as means ± SD. Between-group differences in continuous variables were assessed by univariate analysis using Student *t* test. All calculations were performed with SPSS version 12.0 (SPSS, Chicago, IL).

3. Results

3.1. Effects of the HFD on metabolic parameters

As shown in Table 1, no differences were observed in any parameters between the HFD and control mice after 6 weeks of treatment. After 24 weeks, mice fed the HFD weighed significantly more and had more visceral fat compared with

Table 1
Clinical and biochemical parameters of mice fed the standard chow or HFD after 6 or 24 weeks

Diet type	6 wk		24 wk	
	Control	HFD	Control	HFD
Body weight (g)	25.1 ± 0.9	26.5 ± 1.4	29.0 ± 1.5	35.2 ± 3.8*
Liver weight (g)	1.11 ± 0.09	1.03 ± 0.12	1.28 ± 0.07	1.20 ± 0.23
Retroperitoneal fat pad weight (g)	0.07 ± 0.05	0.10 ± 0.08	0.24 ± 0.09	0.61 ± 0.17**
Plasma triglycerides (mg/dL)	69.1 ± 9.0	75.0 ± 18.9	41.5 ± 9.2	63.0 ± 15.0
Plasma total cholesterol (mg/dL)	85.0 ± 7.4	117.7 ± 37.0	84.6 ± 7.9	132.6 ± 26.1*
Plasma FFAs (mEq/L)	0.60 ± 0.16	0.61 ± 0.21	0.48 ± 0.09	0.54 ± 0.16
Plasma TNF-α (pg/mL)	<10	<10	ND	ND
Fasting plasma insulin (μU/mL)	14.6 ± 3.6	18.1 ± 7.6	15.7 ± 6.2	43.3 ± 14.3*
Hepatic triglycerides (μg/mg protein)	64.8 ± 23.2	73.8 ± 15.4	148.6 ± 46.7	143 ± 43.0
Hepatic total cholesterol (μg/mg protein)	43.0 ± 6.3	40.8 ± 6.0	34.3 ± 4.9	36.5 ± 4.5
Hepatic FFAs (μEq/mg protein)	46.7 ± 6.9	48.8 ± 3.6	53.1 ± 4.0	71.0 ± 7.6*

Values represent the means ± SD of 5 mice per group. ND indicates not determined.
Significantly different from control value: *$P < .05$; **$P < .01$.

control mice. Fasting plasma insulin levels were significantly higher in mice fed the HFD than in control mice. The HFD also induced the accumulation of FFAs in the liver after 24 weeks. These results suggest that mice fed the HFD maintained metabolic homeostasis up to 6 weeks, at which point obesity and insulin resistance developed.

3.2. Effects of the HFD on insulin sensitivity

To evaluate insulin sensitivity, GTT and ITT were conducted after 6 and 24 weeks of treatment in both groups (Fig. 1). Although there was no significant difference in the blood glucose level between the HFD and control mice at 6 weeks, the HFD mice exhibited impaired glucose tolerance (Fig. 1A) and insulin resistance (Fig. 1B) at 24 weeks. These results are consistent with the above observation that obesity, abdominal adiposity, and hyperinsulinemia were induced only after mice were fed the HFD for 24 weeks.

3.3. Fatty acid metabolism pathways are differentially regulated in liver and adipose tissue of mice fed the HFD

We compared liver and adipose tissue gene expression data between mice fed the HFD and control mice after

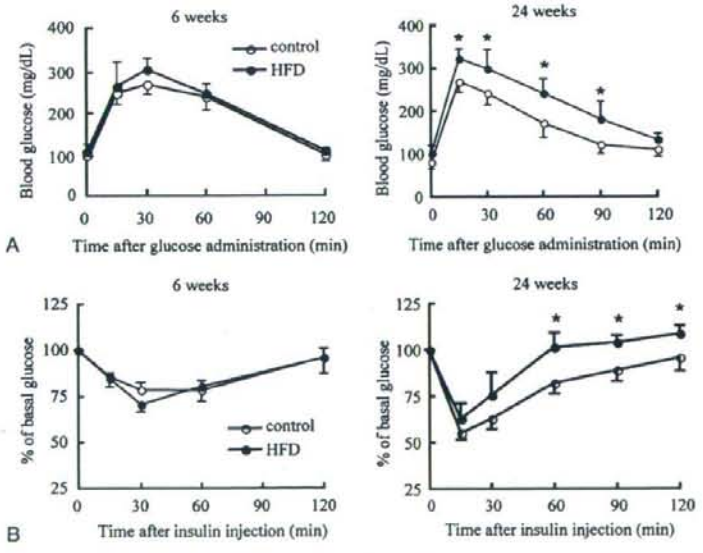

Fig. 1. Evaluation of glucose tolerance and insulin sensitivity. The GTT (A) and ITT (B) after 6 or 24 weeks of standard chow or the HFD. Values represent the means ± SD for 5 mice. *$P < .05$ vs the control group.

6 weeks of treatment to identify pathways with the potential to induce insulin resistance (Table 2). The gene expression levels of various metabolic pathways were already altered at 6 weeks. In particular, pathways for sterol regulatory element binding protein 1c–related fatty acid synthesis (Fig. 2 and Supplementary Fig. 1A) and peroxisome proliferator–activated receptor (PPAR) α–related fatty acid oxidation were up-regulated in the liver of the HFD mice. In contrast, the pathway for fatty acid synthesis was down-regulated in the adipose tissue (Supplementary Fig. 1B). Such compensatory alterations in the expression of genes that regulate fatty acid metabolism seem to help maintain plasma and hepatic levels of FFAs, which have been considered to be a causal factor for insulin resistance [10,11]. In the current study, these levels were similar between the HFD mice and control mice at 6 weeks (Table 1).

3.4. Oxidative stress pathways are coordinately up-regulated in both liver and adipose tissue of mice fed the HFD

In contrast to the pathways for fatty acid metabolism, oxidative stress pathways were coordinately up-regulated in both the liver and adipose tissue (Table 2 and Supplementary Fig. 1C, D). The oxidative stress pathway is composed of genes for ROS production, stress signaling, and antioxidant enzymes. Reactive oxygen species are radical forms of oxygen that can arise from several biochemical reactions: (1) loading of excessive electrons in the respiratory chain by increased mitochondrial fatty acid β-oxidation [12], (2) peroxisomal fatty acid β-oxidation by acyl–coenzyme A oxidase (Acox) [13], (3) microsomal fatty acid ω-oxidaiton by cytochrome P450 2E1 (CYP2E1) [14], and (4) reduction of oxygen by the nicotinamide adenine dinucleotide phosphate (NADPH) oxidase (Nox) complex [15].

To determine the sources of ROS in the liver and adipose tissue of mice fed the HFD, we examined the messenger RNA (mRNA) expression levels of genes involved in ROS production through the use of quantitative real-time PCR (Fig. 2). In the liver of mice fed an HFD for 6 weeks, the expression levels of genes encoding key regulators of mitochondrial fatty acid β-oxidation, including PPARα, carnitine palmitoyltransferase 1a (CPT-1a), Acox1, and CYP2E1, were significantly up-regulated (1.6-, 2.0-, 1.5-, and 1.5-fold, respectively) compared with control mice, whereas the expression levels of Nox2, Nox4, and the Nox complex components $p22^{phox}$ and $p47^{phox}$ were similar between HFD mice and control mice. In the adipose tissue of mice fed an HFD for 6 weeks, gene expression levels of Acox1, CYP2E1, Nox4, and $p22^{phox}$ were significantly up-regulated (1.6-, 1.4-, 2.3-, and 1.6-fold, respectively) compared with control mice; in contrast to the liver, the adipose tissue did not show up-regulated expression of the genes for PPARα and CPT-1a. These results suggest that the source of ROS may differ according to the specific tissue, such that an HFD may induce ROS production in distinctly different manners in the liver and adipose tissue. An HFD may induce ROS production through fatty acid oxidation in the mitochondria of the liver but via Nox in the adipose tissue.

Table 2
Biological pathways of liver or adipose tissue genes regulated by the HFD after 6 weeks

Pathway name	Number of genes changed	Number of genes measured	z score	permuted P value
Liver				
Up-regulated				
Cholesterol biosynthesis	10	15	4.61	<.001
[redacted]	9	14	4.23	<.001
[redacted]	16	38	3.52	.001
Glucocorticoid mineralocorticoid metabolism	7	12	3.39	.006
Statin pathway	9	19	3.06	.005
[redacted]	14	41	2.37	.018
Fatty acid beta oxidation	10	27	2.30	.021
Down-regulated				
Electron transport chain (= respiratory chain)	28	82	4.77	<.001
ACE-inhibitor pathway	5	8	3.72	.003
Adipose tissue				
Up-regulated				
TGF Beta signaling pathway	27	50	3.645	.001
Complement and coagulation cascades	29	59	3.149	.001
Adipogenesis	51	129	2.638	.014
[redacted]	18	38	2.287	.026
Smooth muscle contraction	61	157	2.282	.024
Inflammatory response pathway	18	40	2.018	.037
Down-regulated				
Focal adhesion	74	189	3.50	<.001
Glycolysis and gluconeogenesis	21	41	3.35	<.001
Electron transport chain (= respiratory chain)	35	82	3.01	.002
Krebs-TCA cycle	14	29	2.46	.020
[redacted]	8	14	2.45	.029
Pentose phosphate pathway	5	8	2.19	.038

Pathway analysis was performed using MAPPFinder 2.0 and the Mm-std 20051114.gdb database. The criteria for genes with significantly increased or decreased expression were change-fold (ratio to control) >20% (ie, >1.20 or <0.83). For each pathway, the number of genes that meet the criteria for a significant increase or decrease was determined. This number was compared with the number of pathway genes detected by microarray analysis. These values were used to calculate the *z* score and the permuted *P* value. Pathways indicated by arrows were coordinately regulated between the liver and adipose tissue (retroperitoneal fat). On the other hand, pathways for fatty acid synthesis and glycolysis and gluconeogenesis were up-regulated in the liver (highlighted in dark grey) and down-regulated in adipose tissue (highlighted in light grey).

Oxidative stress is regulated by the balance between ROS production and antioxidant enzyme activity [7]. Consequently, we determined the expression levels of the genes for glutathione peroxidase (Gpx) and Mn–superoxide dismutase, both of which reduce ROS and lipid peroxides, resulting in decreased oxidative stress (Fig. 2). The

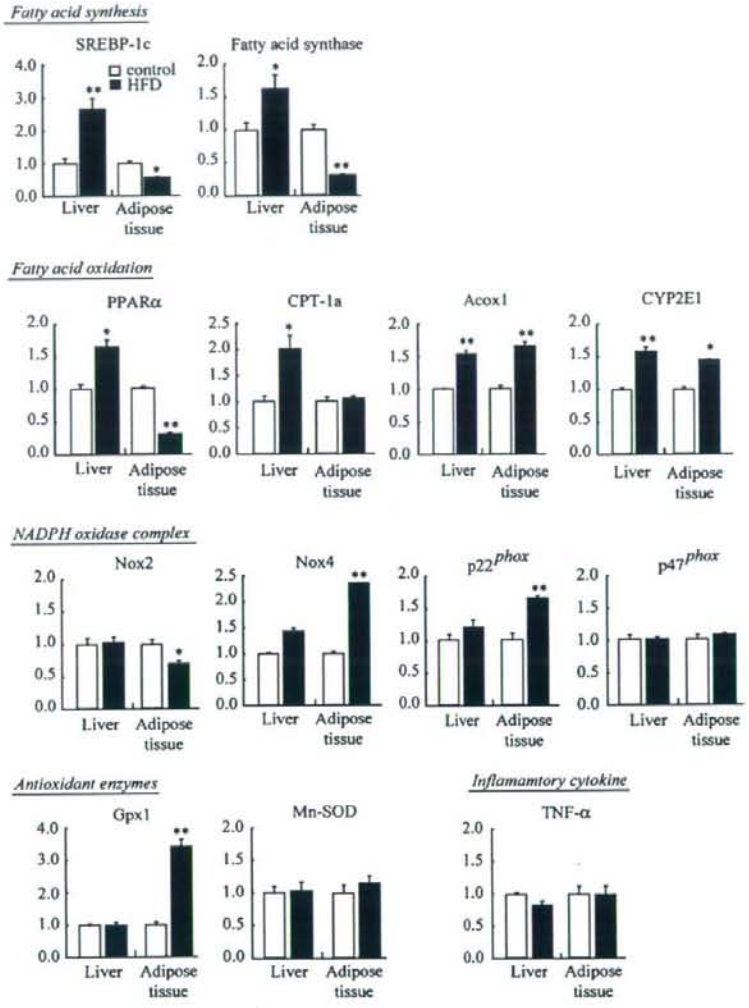

Fig. 2. Quantitative real-time PCR for representative genes involved in fatty acid metabolism and oxidative stress. The mRNA levels of sterol regulatory element binding protein 1c, fatty acid synthase, PPARα, CPT-1a, Acox1, CYP2E1, Nox2, Nox4, $p22^{phox}$, $p47^{phox}$, Gpx1, Mn–superoxide dismutase, and TNF-α in the liver or retroperitoneal fat of mice fed standard chow (n = 3) or the HFD (n = 3) were quantified using real-time PCR after 6 weeks of feeding. The RNA samples for real-time PCR were the same as those for the microarray analysis. Gene expression levels were normalized to 18S ribosomal RNA. The degree of change in gene expression is based on the mean expression level of control mice. Values represent the means ± SD for 3 mice. $^{*}P < .05$ and $^{**}P < .01$ vs the control mice.

expression level of the Gpx1 gene was significantly up-regulated (3.4-fold) in the adipose tissue, but not in the liver, of mice fed the HFD compared with control mice. The insufficient up-regulation of antioxidant enzymes may therefore cause more oxidative stress in the liver than in the adipose tissue.

The proinflammatory cytokine TNF-α, which is elevated in obese rodents and humans, is also an important contributor to the development of insulin resistance [16]. However, the mRNA expression level of TNF-α in the liver and adipose tissue of mice fed the HFD for 6 weeks was similar to that of control mice (Fig. 2). Furthermore, the plasma level of TNF-α was below the detection limit of the enzyme-linked immunosorbent assay (<10 pg/mL) in both groups. These results suggest that the up-regulation of genes for ROS production, rather than the elevation of

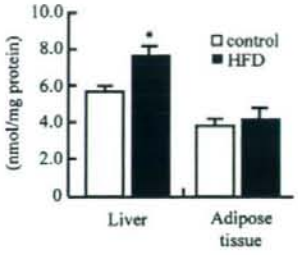

Fig. 3. Measurement of protein carbonyl levels in the liver and adipose tissue. Protein carbonyl concentration was analyzed as a marker for oxidative stress in the liver and retroperitoneal fat. Values represent the means ± SD for 5 mice. $^{*}P < .05$ vs the control mice.

TNF-α, may be an early event triggering insulin resistance in mice fed an HFD.

3.5. Evaluation of oxidative stress in the liver and adipose tissue of mice fed the HFD

To confirm whether high fat intake increases oxidative stress, we measured the protein carbonyl level (marker for cumulative oxidative stress) in the liver and adipose tissue. As expected, the protein carbonyl level was elevated by 35% in the liver but was not altered in the adipose tissue of mice fed the HFD compared with control mice at 6 weeks (Fig. 3). The up-regulation of antioxidant enzymes (ie, Gpx1) in the adipose tissue may compensate for the increase of ROS, lowering oxidative stress.

4. Discussion

Reactive oxygen species production is one of many factors that have been suggested to play a role in the development of insulin resistance, based on the following evidence: (1) high doses of hydrogen peroxide [17] and reagents that accumulate ROS [18] can induce insulin resistance in 3T3-L1 adipocytes, and (2) increased markers of oxidative stress were observed in obese humans [19] and rodents [17,20]. It remains unclear, however, whether increased ROS production causes insulin resistance in vivo. In this study, we demonstrated that the up-regulation of genes responsible for ROS production occurs in both the liver and adipose tissue before the onset of insulin resistance and obesity in mice fed an HFD.

In our dietary model of insulin resistance, the mRNA up-regulation of genes for fatty acid oxidation was observed in the liver. Previous studies have also shown that fatty acid oxidation was increased in the liver to compensate for high fat intake [21]. In addition, pathways involved in the mitochondrial respiratory chain were coordinately down-regulated in both the liver and adipose tissue of mice fed the HFD. These results are consistent with previous reports in skeletal muscle of both humans and mice [22]. High mitochondrial β-oxidation rates seem to help metabolize excess FFAs, although large amounts of electrons entering the respiratory chain may cause abnormal reduction of oxygen. An influx of electrons may then lead to increased mitochondrial ROS production. This suggests that impaired respiratory chain function may cause increased mitochondrial ROS production. Furthermore, we speculate that the down-regulation of the respiratory chain may lead to an influx of FFAs to intracellular peroxisomes and microsomes instead of to mitochondria, resulting in further generation of ROS by Acox and CYP2E1, genes up-regulated in both liver and adipose tissue in this study.

The Nox complex may be a major source of ROS production in adipose tissue but not in liver. Furukawa et al [17] reported that the mRNA expression of Nox2 and its subunits $p22^{phox}$, $p47^{phox}$, and $p67^{phox}$ was significantly up-regulated in the adipose tissue of obese KKAy mice compared with lean C57BL/6J mice. In the present study, however, the HFD up-regulated only Nox4 and $p22^{phox}$ expression in adipose tissue. This discrepancy may be attributed to the difference between genetically and HFD-induced obese models. Given that complexes of Nox4 with $p22^{phox}$ increase in the kidney of diabetic rats [23], excessive nutrients (eg, high fat intake) may also induce ROS production via the Nox4/$p22^{phox}$ complex.

It is striking that increased ROS production preceded the elevated levels of TNF-α and FFAs in the plasma and liver. Although TNF-α and FFAs are thought to cause insulin resistance, our results raise the possibility that ROS trigger the development of insulin resistance, resulting in abdominal obesity and elevated TNF-α and FFAs. In summary, the HFD induced oxidative stress, potentially through the up-regulated expression of genes for ROS production, in the liver and adipose tissue. In addition, these changes occurred before the onset of insulin resistance and obesity. Sources of ROS induced by an HFD may differ between the liver and adipose tissue. These findings suggest that ROS production may be the initial event triggering HFD-induced insulin resistance and therefore may be an attractive therapeutic target for preventing insulin resistance and obesity caused by an HFD.

Acknowledgment

We thank A Katayama and M Nakamura for technical assistance.

Appendix A. Supplementary data

Supplementary data associated with this article can be found, in the online version, at doi:10.1016/j.metabol.2008.03.010.

References

[1] Yamauchi T, Kamon J, Minokoshi Y, Ito Y, Waki H, Uchida S, et al. Adiponectin stimulates glucose utilization and fatty-acid

oxidation by activating AMP-activated protein kinase. Nat Med 2002;8: 1288-95.
[2] Watanabe M, Houten SM, Mataki C, Christoffolete MA, Kim BW, Sato H, et al. Bile acids induce energy expenditure by promoting intracellular thyroid hormone activation. Nature 2006;439:484-9.
[3] Uno K, Katagiri H, Yamada T, Ishigaki Y, Ogihara T, Imai J, et al. Neuronal pathway from the liver modulates energy expenditure and systemic insulin sensitivity. Science 2006;312:1656-9.
[4] Lan H, Rabaglia ME, Stoehr JP, Nadler ST, Schueler KL, Zou F, et al. Gene expression profiles of nondiabetic and diabetic obese mice suggest a role of hepatic lipogenic capacity in diabetes susceptibility. Diabetes 2003;52:688-700.
[5] Gregoire FM, Zhang Q, Smith SJ, Tong C, Ross D, Lopez H, et al. Diet-induced obesity and hepatic gene expression alterations in C57BL/6J and ICAM-1-deficient mice. Am J Physiol Endocrinol Metab 2002;282:E703-13.
[6] Herman MA, Kahn BB. Glucose transport and sensing in the maintenance of glucose homeostasis and metabolic harmony. J Clin Invest 2006;116:1767-75.
[7] Nordberg J, Arner ES. Reactive oxygen species, antioxidants, and the mammalian thioredoxin system. Free Radic Biol Med 2001;31: 1287-312.
[8] Folch J, Lees M, Sloane Stanley GH. A simple method for the isolation and purification of total lipids from animal tissues. J Biol Chem 1957; 226:497-509.
[9] Doniger SW, Salomonis N, Dahlquist KD, Vranizan K, Lawlor SC, Conklin BR. MAPPFinder: using Gene Ontology and GenMAPP to create a global gene-expression profile from microarray data. Genome Biol 2003;4:R7.
[10] Boden G. Role of fatty acids in the pathogenesis of insulin resistance and NIDDM. Diabetes 1997;46:3-10.
[11] Boden G, She P, Mozzoli M, Cheung P, Gumireddy K, Reddy P, et al. Free fatty acids produce insulin resistance and activate the proinflammatory nuclear factor–kappaB pathway in rat liver. Diabetes 2005; 54:3458-65.
[12] St-Pierre J, Buckingham JA, Roebuck SJ, Brand MD. Topology of superoxide production from different sites in the mitochondrial electron transport chain. J Biol Chem 2002;277:44784-90.
[13] Osmundsen H, Bremer J, Pedersen JI. Metabolic aspects of peroxisomal beta-oxidation. Biochim Biophys Acta 1991;1085: 141-58.
[14] Chitturi S, Farrell GC. Etiopathogenesis of nonalcoholic steatohepatitis. Semin Liver Dis 2001;21:27-41.
[15] Krieger-Brauer HI, Kather H. Human fat cells possess a plasma membrane–bound H2O2-generating system that is activated by insulin via a mechanism bypassing the receptor kinase. J Clin Invest 1992;89: 1006-13.
[16] Hotamisligil GS, Shargill NS, Spiegelman BM. Adipose expression of tumor necrosis factor–alpha: direct role in obesity-linked insulin resistance. Science 1993;259:87-91.
[17] Furukawa S, Fujita T, Shimabukuro M, Iwaki M, Yamada Y, Nakajima Y, et al. Increased oxidative stress in obesity and its impact on metabolic syndrome. J Clin Invest 2004;114:1752-61.
[18] Lin Y, Berg AH, Iyengar P, Lam TK, Giacca A, Combs TP, et al. The hyperglycemia-induced inflammatory response in adipocytes: the role of reactive oxygen species. J Biol Chem 2005;280:4617-26.
[19] Urakawa H, Katsuki A, Sumida Y, Gabazza EC, Murashima S, Morioka K, et al. Oxidative stress is associated with adiposity and insulin resistance in men. J Clin Endocrinol Metab 2003;88:4673-6.
[20] Diniz YS, Rocha KK, Souza GA, Galhardi CM, Ebaid GM, Rodrigues HG, et al. Effects of *N*-acetylcysteine on sucrose-rich diet–induced hyperglycaemia, dyslipidemia and oxidative stress in rats. Eur J Pharmacol 2006;543:151-7.
[21] Akbiyik F, Cinar K, Demirpence E, Ozsulhi T, Tunca R, Haziroglu R, et al. Ligand-induced expression of peroxisome proliferator–activated receptor alpha and activation of fatty acid oxidation enzymes in fatty liver. Eur J Clin Invest 2004;34:429-35.
[22] Sparks LM, Xie H, Koza RA, Mynatt R, Hulver MW, Bray GA, et al. A high-fat diet coordinately downregulates genes required for mitochondrial oxidative phosphorylation in skeletal muscle. Diabetes 2005;54: 1926-33.
[23] Etoh T, Inoguchi T, Kakimoto M, Sonoda N, Kobayashi K, Kuroda J, et al. Increased expression of NAD(P)H oxidase subunits, NOX4 and p22phox, in the kidney of streptozotocin-induced diabetic rats and its reversibity by interventive insulin treatment. Diabetologia 2003;46: 1428-37.

Tranilast, an Antifibrogenic Agent, Ameliorates a Dietary Rat Model of Nonalcoholic Steatohepatitis

Masafumi Uno,[1*] Seiichiro Kurita,[1*] Hirofumi Misu,[1] Hitoshi Ando,[1] Tsuguhito Ota,[1] Naoto Matsuzawa-Nagata,[1] Yuki Kita,[1] Satoko Nabemoto,[1] Hiroshi Akahori,[1] Yoh Zen,[2] Yasuni Nakanuma,[2] Shuichi Kaneko,[1] and Toshinari Takamura[1]

Nonalcoholic steatohepatitis (NASH) is the progressive form of nonalcoholic fatty liver disease and is one of the most common liver diseases in the developed world. The histological findings of NASH are characterized by hepatic steatosis, inflammation, and fibrosis. However, an optimal treatment for NASH has not been established. Tranilast, *N*-(3′,4′-dimethoxycinnamoyl)-anthranilic acid, is an antifibrogenic agent that inhibits the action of transforming growth factor beta (TGF-β). This drug is used clinically for fibrogenesis-associated skin disorders including hypertrophic scars and scleroderma. TGF-β plays a central role in the development of hepatic fibrosis, and tranilast may thus ameliorate the pathogenesis of NASH. We investigated the effects of tranilast using an established dietary animal model of NASH, obese diabetic Otsuka Long-Evans Tokushima Fatty (OLETF) rats and nondiabetic control Long-Evans Tokushima Otsuka (LETO) rats fed a methionine-deficient and choline-deficient diet. Treatment with 2% tranilast (420 mg/kg/day) for 8 weeks prevented the development of hepatic fibrosis and the activation of stellate cells, and down-regulated the expression of genes for TGF-β and TGF-β-target molecules, including α1 procollagen and plasminogen activator-1. In addition, tranilast attenuated hepatic inflammation and Kupffer cell recruitment, and down-regulated the expression of tumor necrosis factor alpha. Unexpectedly, tranilast ameliorated hepatic steatosis and up-regulated the expression of genes involved in beta-oxidation, such as peroxisome proliferator–activated receptor α and carnitine *O*-palmitoyltransferase-1. Most of these effects were observed in LETO rats and OLETF rats, which suggest that the action of tranilast is mediated through the insulin resistance–independent pathway. *Conclusion:* Our findings suggest that targeting TGF-β with tranilast represents a new mode of therapy for NASH. (HEPATOLOGY 2008;48:109-118.)

Nonalcoholic fatty liver disease (NAFLD) is one of the most common liver diseases in the United States and other developed countries[1,2] and involves a wide spectrum of liver disease, ranging from simple steatosis to steatohepatitis and cirrhosis. Nonalcoholic steatohepatitis (NASH), the progressive form of NAFLD, is characterized by steatosis, inflammation, and fibrosis. It has recently been proposed that NAFLD be included as a component of the metabolic syndrome, a cluster of metabolic abnormalities with visceral fat accumulation, hyperglycemia, hypertension, and dyslipidemia.[3-5] Insulin resistance, an underlying factor in these metabolic disorders, may play a critical role in the pathogenesis of NASH. We recently created a rat model of NASH with insulin resistance, abundant visceral fat tissue, hyperglycemia, and hypertension, and demonstrated that pioglitazone, a peroxisomal proliferator-activated (PPAR)-γ agonist, prevents the progression of NASH, mainly through enhancement of insulin resistance.[6] However, whether all patients with NASH respond to insulin-sensitizing agents such as PPAR-γ agonists remains unresolved,[7] and the optimal treatment of NASH has not been established.

Transforming growth factor beta (TGF-β) is a multifunctional peptide that plays a pivotal role in fibrogenesis.[8-11] High levels of TGF-β are often found in hepatic fibrosis, and it has been implicated as a mediator of fibro-

Abbreviations: 4-HNE, 4-hydroxynonenal; α-SMA, alpha smooth muscle actin; ALT, alanine aminotransferase; CPT-1, carnitine O-palmitoyltransferase-1; IL-6, interleukin-6; iNOS, inducible NO synthase; LETO, Long-Evans Tokushima Otsuka; LPS, lipopolysaccharide; MCD, methionine- and choline-deficient; mRNA, messenger RNA; NAFLD, nonalcoholic fatty liver disease; NASH, nonalcoholic steatohepatitis; OLETF, Otsuka Long-Evans Tokushima Fatty; PAI-1, plasminogen activator inhibitor-1; PCR, polymerase chain reaction; PPAR, peroxisomal proliferator activated receptor; SEM, standard error of the mean; TGF-β, transforming growth factor beta; TNF-α, tumor necrosis factor alpha; VCAM, vascular cell adhesion molecule.

From the Departments of [1]Disease Control and Homeostasis and [2]Human Pathology, Kanazawa University Graduate School of Medical Science, Kanazawa, Japan.

These authors contributed equally to this work.

Received September 7, 2007; accepted February 20, 2008.

Address reprint requests to: Toshinari Takamura, M.D., Ph.D., Department of Disease Control and Homeostasis, Kanazawa University Graduate School of Medical Science, 13-1 Takara-machi, Kanazawa, Ishikawa 920-8641, Japan. E-mail: ttakamura@m-kanazawa.jp; fax: (81)-76-234-4250.

Copyright © 2008 by the American Association for the Study of Liver Diseases.

Published online in Wiley InterScience (www.interscience.wiley.com).

DOI 10.1002/hep.22338

Potential conflict of interest: Nothing to report.

sis in several liver diseases.[12] TGF-β stimulates collagen synthesis in cultured stellate cells, and hepatic overexpression of TGF-β in transgenic mice has been shown to cause hepatic fibrosis.[13,14] Several lines of evidence have demonstrated that the blockade of TGF-β synthesis or signaling using different experimental strategies prevents liver fibrosis in various animal models.[15-18] TGF-β is also known to play a central role in the development of NASH by activating hepatic fibrosis.[19] Thus, TGF-β signaling can be designated as a potential antifibrogenic target for the treatment of fibrosis-associated liver diseases.

Tranilast, *N*-(3′,4′-dimethoxycinnamoyl)-anthranilic acid, was originally developed as an antiallergic drug for the systemic and topical treatment of bronchial asthma, atopic dermatitis, and allergic conjunctivitis because it inhibits the release of chemical mediators from mast cells and cytokines from macrophages.[8] More recently, tranilast has been reported to exert antifibrogenic effects by inhibiting the action of TGF-β. In fact, tranilast has been used clinically for the treatment of hypertrophic scars, scleroderma, and skin disorders associated with an excessive fibrogenic response.[20,21] We previously found that tranilast prevents renal fibrosis in animal models of diabetic nephropathy, through the suppression of TGF-β.[22] However, no reports are available on the effect of tranilast in animal models of liver diseases.

We therefore hypothesized that the administration of tranilast would exert a beneficial effect on the pathology of NASH by suppressing TGF-β activity and the development of hepatic fibrosis. To test this hypothesis, we investigated the effect of tranilast by using an established dietary animal model of NASH, obese diabetic rats fed a methionine-deficient and choline-deficient (MCD) diet.[6]

Materials and Methods

Animal Model and Experimental Design. Male Otsuka Long-Evans Tokushima Fatty (OLETF) rats, an established animal model of obese type 2 diabetes,[23] were used (Otsuka Pharmaceutical, Tokushima, Japan). Spontaneous-onset type 2 diabetic OLETF rats showed obesity and hyperinsulinemia from 8 weeks of age. NAFLD has been studied in OLETF rats because these animals show an age-dependent increase in fat accumulation in the liver. All rats in the OLETF group developed diabetes after 24 weeks of age (data not shown) as described previously.[23,24] As control animals, 4-week-old OLETF and Long-Evans Tokushima Otsuka (LETO) rats, which originated from the same colony as the OLETF rats by selective mating but do not develop diabetes, were obtained and housed in a room under controlled temperature (25°C), humidity, and lighting (12-hour artificial light and dark cycle). Animals were given free access to standard laboratory rat chow and tap water. At 24 weeks of age, OLETF rats were divided into two experimental groups and fed for 8 weeks as follows: MCD diet (Oriental Yeast, Tokyo, Japan; OLETF-MCD, 21% fat, n = 11), and MCD-tranilast diet (OLETF-MCD-trani; tranilast content 1%, n = 3, 1.4%, n = 3, 2%, n = 10). In addition, at 24 weeks of age, male LETO rats were divided into two groups: MCD diet (LETO-MCD, n = 9) and MCD-tranilast diet (LETO-MCD-trani; tranilast content 2%, n = 5). The rats were allowed unrestricted access to water and the standard or mixed chow. The body weight and food intake in each group of rats were recorded every week. Tranilast was donated by Kissei Pharmaceutical Co. (Matsumoto, Japan). All animal procedures were performed in accordance with the standards set forth in the Guidelines for the Care and Use of Laboratory Animals at the Takara-machi campus of Kanazawa University.

Blood Sampling and Analysis. After 8 weeks, the rats were killed, and blood samples were obtained from the heart after a 12-hour fast. Blood glucose was determined by the Freestyle Kissei monitor (Kissei Pharmaceutical Co). The blood samples were centrifuged, and serum was frozen at −70&°;C for subsequent measurement of serum alanine aminotransferase (ALT), triglyceride, free fatty acid, total cholesterol, and high-density lipoprotein cholesterol levels. Plasma ALT was determined by spectrophotometry (Sigma-Aldrich, St. Louis, MO), according to the manufacturer's instructions. Plasma free fatty acid levels were determined by a nonesterified fatty acid C-test (Wako, Osaka, Japan). Total cholesterol and high-density lipoprotein cholesterol concentrations were quantified by colorimetry, as described previously.[21] Plasma levels of insulin and tumor necrosis factor alpha (TNF-α) were determined by enzyme-linked immunosorbent assay (Mercodia, Uppsala, Sweden and Bender Medsystems, Vienna, Austria).

Measurement of Serum Glucose Levels. Three days before sacrifice, all rats underwent an oral glucose tolerance test after a 12-hour fast. Glucose (2 g/kg) was administered orally. Blood was drawn from a tail vein at 0, 60, and 120 minutes for measurement of serum glucose concentrations.

Measurement of Serum and Liver Triglyceride Levels. After 8 weeks, the rats were killed, and liver weight and triglyceride level were measured. For quantification of the hepatic triglyceride content, the liver was lysed with the buffer in a commercially available kit (TG E-test; Wako).

Morphological Analysis and Immunohistochemistry. After 8 weeks on each diet, the animals were killed

and their livers were fixed in 10% buffered formalin and embedded in paraffin. Severity of hepatic histological changes were assessed by hematoxylin-eosin and Azan staining and blindly scored by a single pathologist. Steatosis, fibrosis, and disease activity were semiquantitatively evaluated according to the standard criteria of grading and staging for NASH, with minor modifications.[25] The degree of steatosis was scored as the percentage of hepatocytes containing lipid droplets. Fibrosis scores were as follows: 1, pericellular and perivenular fibrosis; 2, focal bridging fibrosis; 3, bridging fibrosis with lobular distortion; and 4, cirrhosis. Disease activity was evaluated as the sum of scores (score 0-6) of acinar inflammation (score 0-3) and portal inflammation (score 0-3).

Slides were immunostained with monoclonal mouse anti-human alpha-smooth muscle actin (α-SMA) (Dako, Kyoto, Japan), and anti-rabbit TGF-β (Santa Cruz Biotechnology, Santa Cruz, CA) and ED1 (AbD, SerotecOxford, UK). This was followed by application of the immunoperoxidase technique using an Envision kit (Dako). Peroxidase activity was identified by reaction with 3′,3′-diaminobenzidine (Sigma-Aldrich). Two independent observers with no previous knowledge of the experimental design evaluated each section. Positive staining with anti–α-SMA, anti–TGF-β, or anti-ED1 was expressed as a percentage of the field, using WinROOF version 5.71 (Mitani Shoji, Fukui, Japan).

Real-Time Quantitative Polymerase Chain Reaction. Total RNA was extracted from each liver using the RNeasy Mini Kit (Qiagen, Tokyo, Japan) as described previously.[26] Real-time quantitative polymerase chain reaction (PCR) was performed for TGF-β, α1(I) procollagen (collagen I), plasminogen activator inhibitor-1 (PAI-1), carnitine *O*-palmitoyltransferase-1 (CPT-1), PPAR-α, TNF-α, and vascular cell adhesion molecule (VCAM) 1 messenger RNA (mRNA), using the ABI-Prism 7900 Sequence Detection System (Applied Biosystems, Foster City, CA). The sets of primers and TaqMan probes for collagen I were proprietary to Applied Biosystems (TaqMan Gene Expression Assays product). To control for variation in the amount of DNA available for PCR in the different samples, gene expression of the target sequence was normalized against the expression of an endogenous control, 18S rRNA (TaqMan Control Reagent Kit; Applied Biosystems). The PCR conditions were one cycle at 50°;C for 2 minutes, 95°;C for 10 minutes, followed by 50 cycles at 95°C for 15 seconds and 58°;C for 1 minute.

Western Blot Analysis of 4-Hydroxynonenal–Modified Proteins. Livers were homogenized in radio immunoprecipitation assay lysis buffer containing 50 mM Tris-HCl (pH 7.4), 150 mM NaCl, 1 mM ethylenediaminetetraacetic acid, 1% nonyl phenoxylpolyethoxylethanol, 0.25% deoxycholic acid, and a protease inhibitor cocktail (Roche Diagnostics, Indianapolis, IN). The procedures for western blot analysis have been described previously.[27]

Cell Culture Model and Experimental Design. RAW 264.7 macrophages were grown in Dulbecco's minimum essential medium (Gibco, Carlsbad, CA) supplemented with 10% fetal bovine serum in a humidified atmosphere of 5% CO_2 at 37°C until the cells reached 90% confluence. The cells were treated with 1 μg/mL lipopolysaccharide (LPS; *Escherichia coli* 05:B5, Sigma-Aldrich) and tranilast (30 or 300 μmol/L) for 6 hours. After treatment, total RNA was extracted using an RNeasy Mini Kit as described previously.[26] Real-time PCR was used to quantify gene expression for TNF-α, interleukin-6 (IL-6), and inducible nitric oxide synthase (iNOS). In the next experiment, the cells were treated with tranilast alone (30 or 300 μmol/L) for 6 hours. After treatment, enzyme-linked immunosorbent assay was used to determine the concentrations of IL-6 and TNF-α in the culture medium (R&D Systems, Minneapolis, and Bender Medsystems, Vienna, Austria).

Statistical Analysis. All results are shown as means or means ± standard error of the mean (SEM). Data were analyzed by one-way analysis of variance, and $P < 0.05$ was considered statistically significant. All calculations were performed with SPSS version 11.0 software for Windows (SPSS Inc., Chicago, IL).

Results

Tranilast Was Well Tolerated by Rats Fed the MCD Diet. Spontaneous-onset type 2 diabetic OLETF rats were fed with the MCD diet for 8 weeks. The MCD diet caused intense lobular inflammation and prominent perivenular and pericellular fibrosis in zone 3 of the liver (Fig. 1A, B) as previously described.[6] To ascertain the most effective doses of tranilast, we treated the OLETF-MCD rats with tranilast at three concentrations, 1%, 1.4%, and 2%, which provided average doses of 160, 190, and 420 mg/kg/day, respectively. These are reasonable daily doses for animal experiments, as previously determined.[22,28,29] Tranilast did not affect physical appearance, stool composition, coat maintenance, or food or water intake, which indicated that tranilast was well tolerated. Treatment with tranilast dose-dependently ameliorated liver pathology in MCD-OLETF rats (Fig. 1C). The effects were more prominent in the 2% tranilast-treated group, and we thus performed the following investigations in this group.

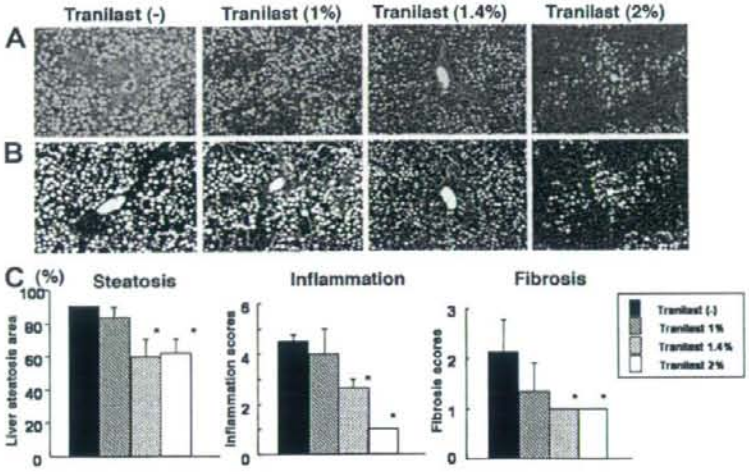

Fig. 1. Tranilast dose-dependently ameliorated liver pathology in OLETF rats fed the MCD diet. Paraffin-embedded sections of the liver were stained with (A) hematoxylin-eosin or (B) Azan stain (original magnification, ×100). (C) Histological changes in the liver were semiquantitatively expressed as histological scores. The MCD diet caused marked macrovesicular steatosis, intense lobular inflammation, and prominent perivenular and pericellular fibrosis in zone 3 of the liver of OLETF rats. Compared with the MCD diet alone, the 1.4% and 2% tranilast-mixed diet significantly improved liver steatosis, fibrosis, and acinar and portal inflammation. Values are means ± SEM. *$P < 0.05$ versus the control diet.

Metabolic Parameters. Metabolic parameters in OLETF rats and nondiabetic control LETO rats fed the MCD diet, with or without 2% tranilast, for 8 weeks are shown in Table 1. Tranilast significantly decreased serum ALT and increased liver weight of both OLETF-MCD and LETO-MCD rats. Blood glucose and triglycerides were unaffected by tranilast. In addition, an insulin loading test showed that tranilast-treated rats exhibited no improvement in insulin sensitivity (data not shown).

Tranilast Inhibited Activation of Stellate Cells and Development of Hepatic Fibrosis in a Dietary Animal Model of NASH. Histological analysis with Azan staining revealed that treatment with 2% tranilast dramatically prevented the development of hepatic fibrosis in LETO-MCD and OLETF-MCD rats (Fig. 2A, B). The activation of hepatic stellate cells is known to play a central role in the development of hepatic fibrosis. Thus, to examine the effect of tranilast on activation of stellate cells, we performed an immunohistochemical analysis of α-SMA, a marker for stellate cell activation. α-SMA–positive cells significantly increased in the liver of OLETF-MCD rats compared with that in LETO-MCD rats. Tranilast reduced the numbers of these cells in both LETO-MCD and OLETF-MCD rats (Fig. 2C, D).

Tranilast Prevented Development of Hepatic Steatosis. Little has been reported on the effect of tranilast on intracellular lipid accumulation. However, unexpectedly, our histological analysis showed that treatment with tranilast clearly improved hepatic steatosis in both LETO-MCD and OLETF-MCD rats (Fig. 3A). Consistent with these histological findings, tranilast significantly reduced hepatic triglyceride content in these two groups of rats (Fig. 3B).

Tranilast Suppressed TGF-β Expression in the Liver in the Dietary Animal Model of NASH. To clarify the mechanism by which tranilast prevents hepatic

Table 1. Effects of MCD and MCD+Tranilast Diets on Metabolic Parameters at 8 Weeks of Treatment

	OLETF		LETO	
Treatment	(−)	Tranilast (2%)	(−)	Tranilast (2%)
Body weight (g)	402 ± 5.4	359 ± 4.5*	384 ± 4.6†	366 ± 6.7
Food intake (kcal/day)	31.1 ± 2.9	36.5 ± 7.1	43.7 ± 1.7†	41.6 ± 0.8†
Tranilast intake (mg/kg HW/day)	(−)	423 ± 99	(−)	482 ± 21
Liver weight (g)	14.2 ± 0.3	15.8 ± 0.5*	9.9 ± 0.4†	12.6 ± 0.2*†
Serum glucose (fasting) (mg/dL)	107 ± 7.1	138 ± 5.0	118 ± 9.6	122 ± 4.1‡
60 min (mg/dL)	222 ± 24.3	238 ± 30.0	172 ± 8.6	150 ± 5.6
120 min (mg/dL)	166 ± 16.9	246 ± 43.8	141 ± 6.0	144 ± 8.2†
Plasma ALT levels (U/L)	165 ± 22.1	80.8 ± 9.9*	118.4 ± 11.0	59.2 ± 3.2*
Serum TNF-α levels (pg/mL)	4.0 ± 3.0	Unmeasurable	0.8 ± 0.7	Unmeasurable

Note. Data are means ± SEM ($n = 9$–11).
*$P < 0.05$ versus rats fed the MCD diet.
‡$P < 0.05$ versus the OLETF rats.